Monthly Notices of the ROYAL ASTRONOMICAL SOCIETY

MNRAS **523,** 4365–4380 (2023) https://doi.org/10.1093/mnras/stad1721
Advance Access publication 2023 June 9

Constraining the atmospheric elements in hot Jupiters with Ariel

Fang Wang,[1,2,3]★ Quentin Changeat ,[3,4] Giovanna Tinetti,[3] Diego Turrini[5,6] and Sam O. M. Wright[3]

[1]*Xi'an Institute of Optics and Precision Mechanics of CAS, 710119 Xi'an, China*
[2]*University of Chinese Academy of Sciences, 100049 Beijing, China*
[3]*Department of Physics and Astronomy, University College London, Gower Street, London, WC1E 6BT, UK*
[4]*European Space Agency (ESA), ESA Office, Space Telescope Science Institute (STScI), 3700 San Martin Drive, Baltimore, MD 21218, USA*
[5]*INAF-Osservatorio Astrofisico di Torino, Via Osservatorio 20, I-10025 Pino Torinese (TO), Italy*
[6]*INAF-Istituto di Astrofisica e Planetologia Spaziali, Via del Fosso del Cavaliere 100, I-00133 Rome, Italy*

Accepted 2023 June 5. Received 2023 May 12; in original form 2022 November 22

ABSTRACT

One of the main objectives of the *European Space Agency's Ariel* telescope (launch 2029) is to understand the formation and evolution processes of a large sample of planets in our Galaxy. Important indicators of such processes in giant planets are the elemental compositions of their atmospheres. Here we investigate the capability of Ariel to constrain four key atmospheric markers: metallicity, C/O, S/O, and N/O, for three well-known, representative hot-Jupiter atmospheres observed with transit spectroscopy, i.e. HD 209458b, HD 189733b, and WASP-121b. We have performed retrieval simulations for these targets to verify how the planetary formation markers listed above would be recovered by Ariel when observed as part of the Ariel Tier 3 survey. We have considered eight simplified different atmospheric scenarios with a cloud-free isothermal atmosphere. Additionally, extra cases were tested to illustrate the effect of C/O and metallicity in recovering the N/O. From our retrieval results, we conclude that Ariel is able to recover the majority of planetary formation markers. The contributions from CO and CO_2 are dominant for the C/O in the solar scenario. In a C-rich case, C_2H_2, HCN, and CH_4 may provide additional spectral signatures that can be captured by Ariel. In our simulations, H_2S is the main tracer for the S/O in hot-Jupiter atmospheres. In the super-solar metallicity cases and the cases with C/O $>$ 1, the increased abundance of HCN is easily detectable and the main contributor to N/O, while other N-bearing species contribute little to the N/O in the investigated atmospheres.

Key words: astrochemistry – instrumentation: spectrographs – planets and satellites: atmospheres – planets and satellites: composition.

1 INTRODUCTION

The detection and characterization of extrasolar planets have become one of the most popular topics in astronomy, with now more than 5000 confirmed exoplanets. The transit method is arguably the most prolific approach for detecting exoplanets. Transit spectroscopy is also being used to study the composition of exoplanet atmospheres: when the stellar light passes through the atmosphere of a transiting planet, additional absorption from the molecules in the planetary atmosphere may occur. This absorption, happening at specific wavelengths, encodes the properties of the planetary atmosphere, which can then be extracted from observations (e.g. Brown 2001).

To date, the most studied atmospheres are the ones of hot-Jupiters, due to the larger spectral features that are imprinted in their spectra and the limitation of current instruments. In particular, HD 209458b and HD 189733b are by far the most studied examples of 'hot-Jupiters', due to their bright host stars and large transit depths, and are here taken as benchmark exoplanets for our study. WASP-121 b is also considered in our simulations.

HD 209458b is the first transiting exoplanet to have been detected (Charbonneau et al. 1999; Henry et al. 1999). A number of molecules have been identified in its transit or eclipse spectra, including H_2O (Swain et al. 2009; Deming et al. 2013; Sing et al. 2016; Tsiaras et al. 2016; Changeat et al. 2022), CO (Snellen et al. 2010; Brogi & Line 2019), CH_4 and CO_2 (Swain et al. 2009), and NH_3 (MacDonald & Madhusudhan 2017). Ions and atoms, such as ionized iron (Fe +; Cubillos et al. 2020) and atomic magnesium (Mg I; Vidal-Madjar et al. 2013), as well as H I, O I, and C II (Vidal-Madjar et al. 2004), were suggested to explain *Hubble Space Telescope*'s data. Giacobbe et al. (2021) estimated a high C/O value in HD 209 458 b's atmosphere using multiple molecules as tracers (H_2O, CO, HCN, C_2H_2, CH_4, and NH_3). Similarly, studies on the molecular composition of the atmosphere on HD 189 733 b (Bouchy et al. 2005) indicate evidence for the presence of H_2O (Tinetti et al. 2007; Swain, Vasisht & Tinetti 2008; Madhusudhan & Seager 2009; Birkby et al. 2013), CO (Swain et al. 2009; de Kok, R.J. et al. 2013), HCN (Cabot et al. 2018) and CH_4 (Swain et al. 2009), sodium (Wyttenbach et al. 2015), and potentially potassium (Keles et al. 2019). Studies about WASP-121b's atmosphere have suggested the presence of a number of atmospheric absorbers, including gaseous Fe (Gibson et al. 2020), Mg (Sing et al. 2019; Hoeijmakers et al. 2020), H_2O (Evans et al. 2016), Cr, V (Ben-Yami et al. 2020), VO (Evans et al. 2018), and

★ E-mail: wangfang16@mails.ucas.ac.cn

Ca (Merritt et al. 2021), and the planet was also recently observed with *James Webb Space Telescope* (*JWST*; Mikal-Evans et al. 2023).

Although a number of studies have been carried out on the molecular and ionic composition in the atmospheres of these three hot-Jupiters, the quantification of the abundances of each species has remained difficult, with many studies finding inconsistent values. Today, there is therefore no consensus on definitive values for the C/O, N/O, and S/O ratios in the atmospheres of those planets. Constraining those ratios, however, is crucial as they might be the most direct outcome of planetary formation and evolution processes (Öberg, Murray-Clay & Bergin 2011; Mordasini et al. 2016; Eistrup, Walsh & van Dishoeck 2018; Cridland, Eistrup & Van Dishoeck 2019; Nowak et al. 2020; Turrini et al. 2021, 2022; Biazzo et al. 2022; Knierim, Shibata & Helled 2022; Kolecki & Wang 2022; Pacetti et al. 2022).

Data from the recently launched NASA/ESA/CSA *JWST* (Greene et al. 2016) suggest that this observatory will play an important role in constraining the elemental ratios in the atmospheres of hot-Jupiters (The JWST Transiting Exoplanet Community Early Release Science Team et al. 2022). However, to constrain planet formation and evolution models, the observation of a large sample of planets is required, which can only be done with a dedicated space instrument, rather than with the multipurpose telescopes that are in operation currently (Wang et al. 2021). The *ESA Ariel* space telescope (Tinetti et al. 2018) is a dedicated survey mission for characterizing the atmosphere of a large sample of exoplanets with transit, eclipse, and phase-curve spectroscopy. Ariel is the M4 mission of the European Space Agency that will be launched to L2 in 2029 (Tinetti et al. 2021) and will have a wavelength coverage from the visible to the mid-infrared. Ariel will simultaneously cover a spectral range from the visible to the mid-infrared (Tinetti et al. 2021) through two instruments. The InfraRed Spectrometer (AIRS) provides spectra with wavelength coverage $\lambda = 1.95$–$7.8\ \mu$m at a spectral resolution (R) of 30–100. The Ariel FGS is used for both pointing and as optical instrument, covering the visible and NIR spectral window through three photometric channels (0.5–1.1 μm) and a low resolution spectrometer ($\lambda = 1.1$–$1.95\ \mu$m). The mission adopts an observational strategy in tiers (from 1 to 4) which tailor the required signal-to-noise ratio (SNR) and resolution to the scientific objectives and type of targets (Edwards et al. 2019; Edwards & Tinetti 2022).

Here we investigate the capability of Ariel to detect elemental ratios in the atmospheres of hot-Jupiters. Previous studies have focused on other scientific objectives of the mission. For example, Changeat et al. (2020) have showed the possibility of recovering chemical trends in a large sample of hydrogen-rich planets observed by Ariel. Other studies (Bourgalais et al. 2020; Changeat et al. 2021a) have focused on the capability of Ariel to observe low-mass planets. Due to the sample nature of the mission, which plans to observe spectroscopically about 1000 exoplanet atmospheres, significant work has also been achieved in the development of fast and reliable techniques to recover information from observed spectra, adopting for instance machine-learning techniques (Yip et al. 2021; Changeat & Hou Yip 2022) or other statistical methods (Mugnai et al. 2021).

To investigate the capability of the *Ariel* telescope to constrain the abundances of atmospheric elements [specifically C/O, S/O, N/O, and metallicity (Tinetti et al. 2021; Turrini et al. 2021, 2022; Pacetti et al. 2022)] using transit spectroscopy, we simulate observations of HD 209 458 b, HD 189 733 b, and WASP-121 b (as three examples of hot Jupiters) in eight different atmospheric environments when multiple transits (5 or 20 times) are combined. In Section 2 we describe our approach. In Section 3 we present the results of our retrievals. In Section 4 further information is discussed and we provide additional experiments to explore the case of N/O. Finally, in Section 5, we draw conclusions from the work above.

Table 1. Parameters of three exoplanetary systems adopted in the forward models.

Characteristics	HD 209 458 b	HD 189 733 b	WASP-121 b
Planet mass (M_J)	0.682	1.166	1.157
Planet radius (R_J)	1.359	1.119	1.753
Planet distance (AU)	0.04707	0.03106	0.02596
Orbital period (day)	3.52475	2.21858	1.27493
T_p (K) (isothermal)	1450	1210	2720
He/H ratio	0.0204	0.0081	0.17
Stellar type	F9	K2	F6
T_s (K)	6065	5050	6400
Stellar radius ($R_\odot$)	1.155	0.765	1.458
Stellar mass ($M_\odot$)	1.119	0.812	1.358
Stellar brightness	V = 7.63	V = 7.65	V = 10.51

2 METHOD

2.1 Overview

To evaluate the capability of the Ariel telescope to constrain elemental ratios in the atmospheres of hot Jupiters, we performed a retrieval analysis of element-to-O ratios and metallicity in eight different scenarios with 5 and 20 observations for the three benchmark planets HD 209 458 b, HD 189 733 b, and WASP-121 b. We used the open-source code TAUREX 3 (Al-Refaie et al. 2021) to generate forward spectra and to perform the inverse spectral retrievals for our different cases. TAUREX 3 is a fully Bayesian retrieval framework, which is simple to use as a library, or standalone program. It provides relevant classes and functions with the advantages of high speed, modularization, high performance, and flexibility.

To understand the potential of Ariel in constraining C/O, N/O, S/O, and metallicity we follow a three-stage process adopted in Changeat et al. (2019). First, we produce a high-resolution (R = 15 000) forward model for each scenario considered to produce the simulated spectra. Secondly, we convolve the high-resolution spectrum with noise simulations for our three planets, produced by the official noise simulator ArielRad (Mugnai et al. 2020), to create simulated observed data with an instrumental resolution. Finally, we use TAUREX 3 in retrieval mode and with large un-informative priors to recover the information content in the simulated telescope observation. The outputs of TAUREX 3 include fitted spectra, atmospheric properties, posteriors distributions, and statistical metrics, which we use to assess the results.

2.2 Forward model assumptions

As previously said, HD 209 458 b, HD 189 733 b, and WASP-121 b are simulated, and the characteristics of these systems are described in Table 1 based on Bonomo et al. (2017), Addison et al. (2019), and Bourrier et al. (2020). In particular, the H/He ratio of HD 209 458 b should be larger than 90/10 according to Lampón et al. (2020). So we set a most likely approximately value of 0.0204 as the He/H ratio for HD 209 458 b, while 0.0081 for HD 189 733 b derived from the research of Lampón et al. (2021) and He/H = 0.17 for WASP-121 b (Cabot et al. 2020).

Table 2. Summary of eight atmospheric scenarios.

	Scenarios	C/O	N/O	S/O	Metallicity
1	Basic solar	0.55	0.14	0.028	1
2	C-rich	1.1	0.14	0.028	1
3	C-poor	0.2	0.14	0.028	1
4	N-rich	0.55	2	0.028	1
5	S-rich	0.55	0.14	0.05	1
6	Low Z	0.55	0.14	0.028	0.5
7	High Z	0.55	0.14	0.028	7.6
8	Very high Z	0.55	0.14	0.028	50

To simulate those spectra, we account for molecular absorption, Collision Induced Absorption (CIA) of H_2-H_2 and H_2-He (Richard et al. 2012), and Rayleigh scattering. For this work, we do not include the effect of clouds, which will be discussed in future works. The atmosphere is discretized in a grid of 100 layers from 10^{-6} Pa to 10^{8} Pa equally spaced in log scale, and an isothermal temperature profile is utilized. We included absorption of 17 molecules using cross-section sampled at a spectral resolution of 15 000: HCN (Barber et al. 2013; Chubb et al. 2021), H_2CO (Al-Refaie et al. 2015), CH_3 (Adam et al. 2019), CH_4 (Yurchenko et al. 2017), CO (Li et al. 2015), CO_2 (Yurchenko et al. 2020), CS (Paulose et al. 2015), C_2H_2 (Chubb, Tennyson & Yurchenko 2020), C_2H_4 (Mant et al. 2018), OH^+ (Hodges & Bernath 2017; Bernath 2020), SH (Gorman, Yurchenko & Tennyson 2019), H_2O (Polyansky et al. 2018), H_2S (Azzam et al. 2016), NH_3 (Coles, Yurchenko & Tennyson 2019), NO (Wong et al. 2017; Qu, Yurchenko & Tennyson 2021), NS (Yurchenko et al. 2018), and SO_2 (Underwood et al. 2016). They are chosen for their potential influence on the C/O, N/O, S/O, and metallicity.

To model the chemistry of those atmospheres, we utilized the equilibrium chemistry plugin FastChem (Stock et al. 2018; Al-Refaie et al. 2022b). For this work, we include H, He, C, N, O, and S species and recover elemental abundances as element-to-O ratios (C, N, and S) and metallicity.

Eight physical scenarios inspired by the literature are simulated. In this study, we vary only one compositional parameter between any two scenarios to draw a clearer picture of their impact on the atmospheric retrieval. Future studies will need to assess the impact of changing multiple compositional parameters at the same time. We describe those experiments below, while the summary and chosen values for the parameters are shown in Table 2.

(1) A basic solar-abundance scenario. Here we adopt a purely solar composition for the giant planets, both in terms of metallicity and elemental ratios. The solar composition is adopted from Turrini et al. (2021) based on results from Asplund et al. (2009) and Scott et al. (2015a, b).

(2) The C-rich atmosphere scenario. Madhusudhan (2012) and Moses et al. (2012) studied the influence of the C/O ratio on the chemical composition of hot Jupiter atmospheres, and their research indicated that a model with a C/O ratio ∼1 might be indeed possible in exoplanet atmospheres. Specifically, values of the C/O ratio greater than one are associated to giant planets accreting their heavy elements from the disc gas in protoplanetary discs that inherited their volatiles from the interstellar medium through the star formation process (Turrini et al. 2021; Pacetti et al. 2022; Turrini et al. 2022). The observations of HD 209 458 b suggest that the atmospheric C/O ratio could be close to or greater than 1 (Giacobbe et al. 2021). Here, we use C/O $= 1.1$ for our C-rich case, as in the study from Venot et al. (2015), with the other parameters remaining solar.

(3) The C-poor atmosphere scenario. If protoplanetary discs undergo sufficient heating, e.g. by stellar flares or by the native cluster of their host star, their chemistry can be reset, resulting in drastically different C/O ratios of their gas (Eistrup, Walsh & Van Dishoeck 2016; Turrini et al. 2022). Giant planets forming in such environments can be characterized by sub-stellar values of their C/O ratio down to values of 0.2–0.3 (Pacetti et al. 2022). Water-rich planetesimals could also deliver a large quantity of oxygen therefore we explore a possible value of C/O $= 0.2$ in this C-poor scenario.

(4) The N-rich atmosphere scenario. Heng & Tsai (2016) presented novel equilibrium-chemistry formulae for the abundances of molecules in hot exoplanetary atmospheres including the carbon, oxygen, and nitrogen networks, and validated the accuracy of the solutions. As set in their scenarios, the N/O mixing ratio could be defined as 2.0 in the N-rich case, which would be adopted in our scenario. Such high values of the N/O ratio are plausible for giant planets forming in protoplanetary discs that underwent chemical reset if they accrete large quantities of N-rich/O-poor gas, e.g. as in the disc region between the O_2 and N_2 snowlines (Pacetti et al. 2022).

(5) The S-rich atmosphere scenario. In the work of Thompson et al. (2021), theoretical constraints on the initial chemical composition were provided by measuring the abundances of volatiles released from meteorites. They concluded that the S/O ratio could be up to 0.05 for initial bulk CM chondrite composition. In the case of giant planets, the final S/O ratio will depend on the balance between the accretions of chondritic solids and disc gas, as both disc components contribute O to the planets (Turrini et al. 2021; Pacetti et al. 2022). S/O values as high as those reported by Thompson et al. (2021) are plausible for giant planets forming in discs that underwent chemical reset when they obtain their heavy elements from chondritic solids inside the NH_3 snowline (Pacetti et al. 2022). Here, we explore a solar-abundance scenario with a slightly enriched sulphur ratio of 0.05.

The (6) low, (7) high, and (8) very high metallicity scenarios. Measurements of elemental ratios in solar system planets suggest that planetary formation processes lead to super-solar atmospheric metallicity (Owen & Encrenaz 2003; Marty et al. 2009; Mousis et al. 2018; Shibata & Helled 2022). The atmospheric metallicity for hot Jupiters could be several times the solar one (Shibata, Helled & Ikoma 2020, 2022), with Neptune-like planets reaching up to two orders of magnitude higher abundances in heavy elements. Turrini et al. (2021) have shown that values from 0.5 to 7.6 are reasonable with values as low as 0.2 being possible. On top of those two additional cases, we also investigate a 50× solar metallicity case, following (Blumenthal et al. 2018). It's worth pointing out that such a high metallicity value has critical implications for the nature of the giant planet, which makes it more similar to a giant Neptune than to Jupiter.

2.3 Observation spectra simulations

To simulate the Ariel observations, we convolve the high-resolution transit spectra generated by TAUREX 3 with the instrument noise simulator ArielRad (Mugnai et al. 2020). We estimate the spectra at Ariel's Tier-3 resolution (Tinetti et al. 2021). For those observations, the spectral resolution is R $= 20$ for $1.1 < \lambda < 1.95$ μm, R $= 100$ for $1.95 < \lambda < 3.90$ μm, and R $= 30$ for $3.90 < \lambda < 7.80$ μm.

The studies from Feng et al. (2018) and Changeat et al. (2019, 2020) have shown that unscattered spectra are required to keep track of the true values when investigating retrievals biases and correlations from theoretical studies, so for the purposes of our study, we chose not to scatter observations. Note that scattered cases were also investigated as part of this study. The retrieval results for a

Table 3. Free parameters and their priors in the retrievals.

Parameters	Priors	Mode
Planet radius	[0.9, 2.0]	Linear
T	[300.0, 3000.0]	Linear
Metallicity	[−2.0, 3.0]	Log
C/O ratio	[0, 2.0]	Linear
N/O ratio	[0, 2.5]	Linear
S/O ratio	[0, 0.2]	Linear

solar atmosphere in HD 209 458 b are presented in Fig. A1 for five noise instances, demonstrating the robustness of our analysis to the observation scatter.

Here, the noise is considered to follow a normal distribution, so we use $\sigma_N = \sigma/\sqrt{N_t}$, where σ is the noise of a single-observation and N_t is the number of transits to combine multiple transit realizations and obtain σ_N, the noise of N stacked observations. For all three hot Jupiter and in all of our scenarios, we simulated observational data for $N_t = 5$ and 20.

2.4 Retrieval model assumptions

To sample the parameter space and evaluate the ability of Ariel to recover the metallicity, C/O, N/O, and S/O, we use the MultiNest algorithm (Feroz, Hobson & Bridges 2009). MultiNest is a Nested Sampling tool that has been widely used to solve inverse problems by the astrophysical community. For each of the 16 cases (eight scenarios with two N_t), we fitted the simulated observation spectra with evidence tolerance of 0.5 and 300 live points.

For each retrieval, the free parameters are fitted using non-informative uniform priors. Those are listed in Table 3. Due to the wide range of values for metallicity, we fit this parameter in log space.

3 RESULTS

The retrieved spectra and simulated observations of all scenarios are shown in Fig. 1, panels represent the observations for HD 209 458 b with 20 transits, HD 209 458 b with 5 transits, HD 189 733 b with 5 transits, and WASP-121 b with 5 transits, respectively. In general, it can immediately be seen that the different scenarios we consider produce different spectral shapes, which we should be able to recover via our retrieval strategy. For instance, the C-rich case with C/O = 1.1 shows a totally different regime, which would be easy to distinguish from the other cases.

The posterior distributions comparing the results of each scenario are shown as corner plots (Foreman-Mackey 2016), in Fig. 2 for HD 209 458 b with five transits. We show the three other cases (20-transit HD 209 458 b, 5-transit HD189733 b, and 5-transit WASP-121 b) in the Appendix (see Figs B1, B2, and B3, respectively). Overall, the change in the number of observations does not affect the result, but can make the retrieved parameters more precise. This is shown in the median and 1σ credible ranges of retrieved parameters, see Table C1.

From the posterior distributions, most of the considered atmospheric parameters for all three hot Jupiters are well retrieved from Ariel observations. The selected nominal 5 and 20 observations guarantee an excellent SNR for all the planets studied. In the next sections we will discuss in detail the retrievability of the different elemental ratios.

3.1 Metallicity

In all the scenarios, we are able to constrain very accurately the metallicity of the observed hot Jupiters' atmospheres. However, we find a strong degeneracy between the metallicity and C/O ratio for the C-rich atmosphere. This is likely due to the decrease in water abundance, which usually provides an important constraint on oxygen abundance.

3.2 C/O ratio

A similar conclusion can be drawn for the C/O ratio. The cases combining five transits are well retrieved, in spite of demonstrating slightly less accurate constraint than 20-observation cases. To analyse in more detail the effect of species abundance on the C/O ratio, we break down the simulations of HD 209 458 b, providing the mixing ratios profiles of active molecules for the solar scenario and the C-rich scenario in Fig. 3, and the spectral contributions of each species to the absorption spectra are shown in the top and the top middle panels of Fig. 4.

The elemental abundances of carbon are correctly identified due to the distinct absorption characteristics of 5 carbon-related molecules. In the solar case, CO and CO_2 are the main species of interest. In the C-rich case, additional absorption of CH_4, C_2H_2 and HCN can contribute to the direct estimation of the carbon abundance. H_2CO, CH_3, CS, and C_2H_4, remain in low abundance, which does not allow to capture their signature. The increased abundances of HCN, C_2H_2, and CH_4 in C-rich atmospheres were also mentioned in prior studies such as Moses et al. (2012) and Madhusudhan (2012).

(i) CH_4, despite not being the main C-bearing species in hot Jupiter's atmospheres, has strong spectral signatures that allow its detection. Due to the CO to CH_4 conversion reaction which favors CO at temperatures higher than 800K, it is not present in high abundances for the solar case but at C/O $>$ 1, CH_4 becomes abundant and can easily be detected. CH_4 is thought to be of significant importance in cool to warm exoplanets.

(ii) The mixing ratios of HCN and C_2H_2 increase significantly with increasing C/O ratio, and those molecules have strong spectral features in the Ariel range. HCN has strong features at 1.5, 2.5, 3.3, 4 μm, as well as in the range redder than 5 μm. HCN is present in hot atmospheres, but we highlight that this tracer would not be relevant for cooler planets. C_2H_2 appears to be a dominant contribution to the transmission spectrum at 3.3, 3.9, and $\geq$ 5.8 μm.

(iii) CO is the main carbon-bearing species in hot Jupiters with temperatures larger than 1000 K. With prominent absorption peaks at the characteristic wavelengths of 1.5, 2.5, and 5.0 μm, it is an important species to determine the carbon abundance. However, the molecular mixing ratio does not change much with the changes in C/O and its molecular features often overlap with other molecules.

(iv) CO_2 has characteristic signatures around 2.0, 2.9, and 4.5 μm, which can easily be picked up by Ariel. As it requires two oxygen atoms, carbon dioxide abundance decreases with increasing the C/O ratio, making it a very good tracer for the C/O ratio.

(v) CS, CH_3, and C_2H_4 have slightly increased abundances, but their contributions to the transit spectra remain marginal.

3.3 S/O ratio

The S/O ratio is well constrained in the cases of HD 209 458 b and HD 189 733 b but not for WASP-121 b, even in the S-rich case. Compared to the two other exoplanets, the contribution of H_2S in WASP-121 b is diminished. This is due to the higher

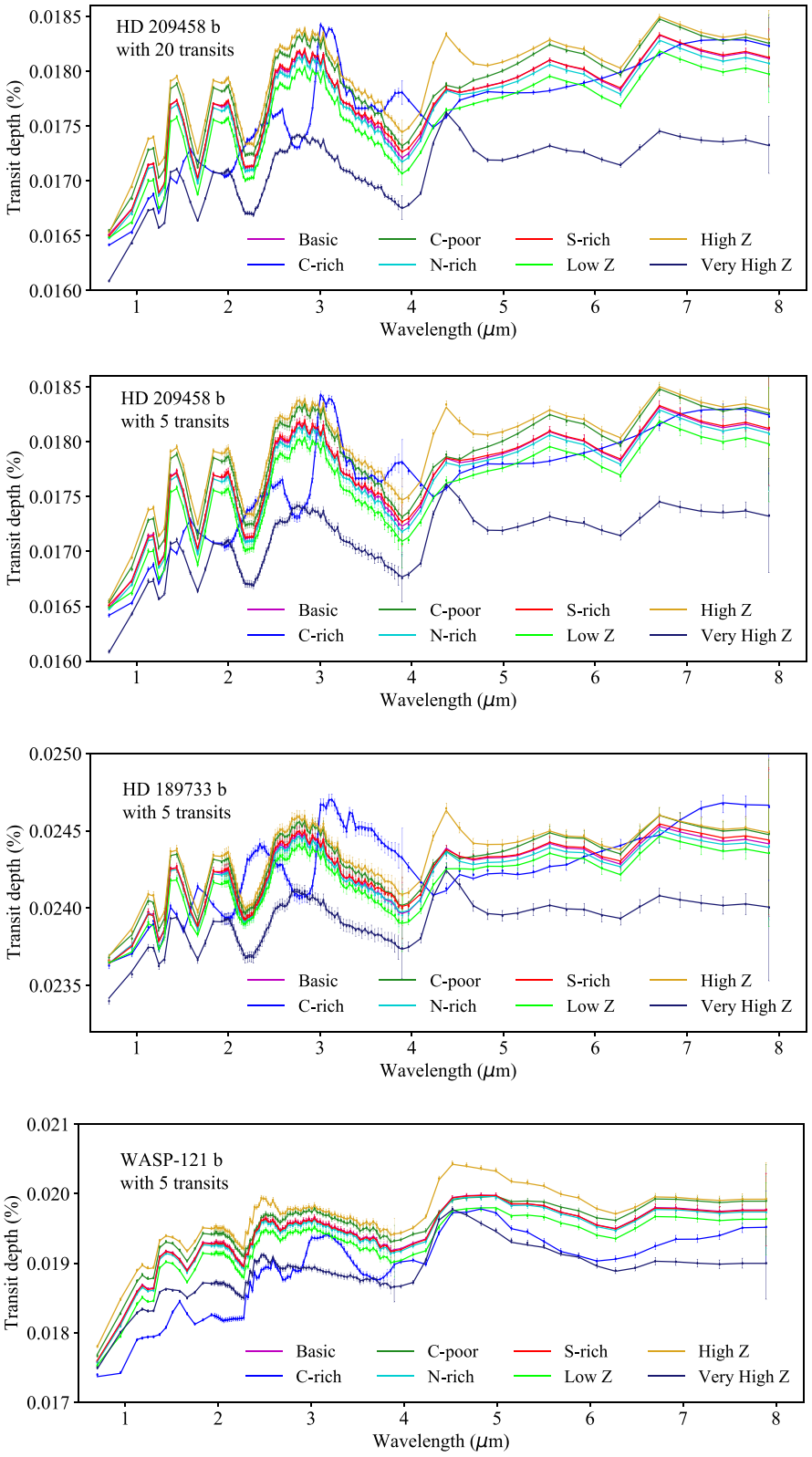

Figure 1. Simulated transit spectra as observed by Ariel for the three selected hot-Jupiters, and eight atmospheric scenarios. Top panel: Transit spectra of HD 209 458 b obtained by combining 20 transits. Top middle panel: transit spectra of HD 209 458 b obtained by combining five transits. Bottom middle panel: Transit spectra of HD 189 733 b obtained by combining five transits. Bottom panel: Transit spectra of WASP 121 b obtained by combining five transits. Note that non-scattered spectra are used for all of the retrievals.

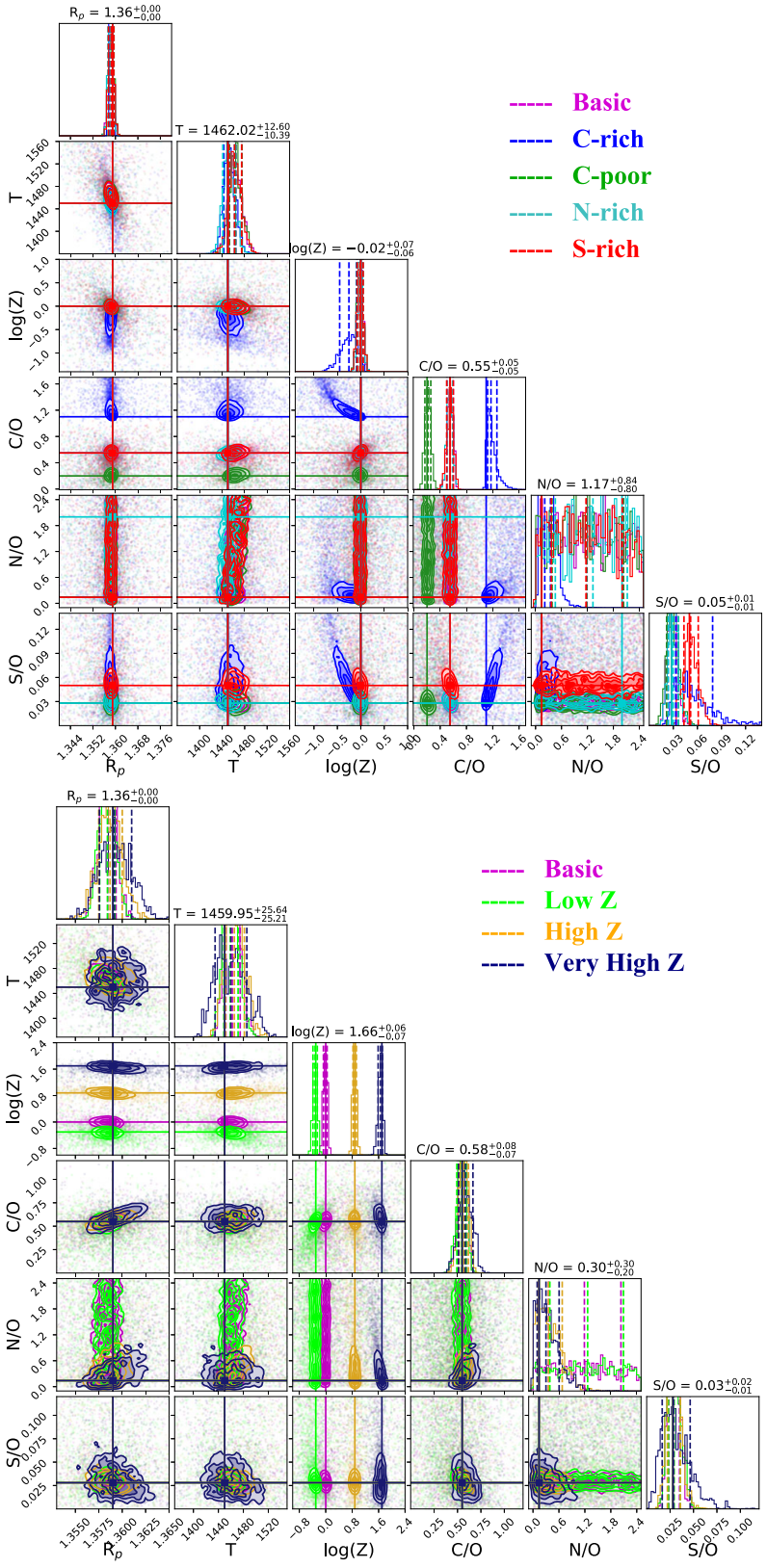

Figure 2. Posterior distributions of the eight scenarios considered for HD 209 458 b when five transit observations obtained by Ariel are combined (top middle panel in Fig. 1). Scenarios 1, 2, 3, 4, and 5 are shown in the top plot, while scenarios 1, 6, 7, and 8 in the bottom plot. The true values assumed in the forward models are indicated as solid lines, dashed lines mark the median values of the free parameters, and the $\pm\sigma$ uncertainties.

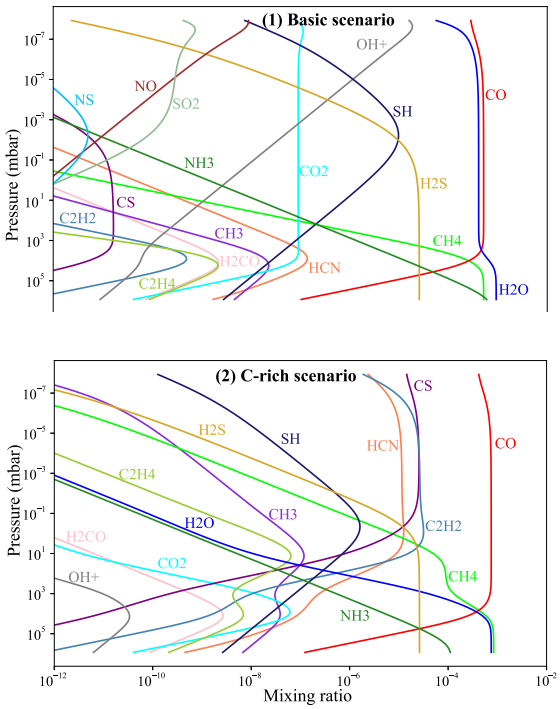

Figure 3. Vertical abundance profiles of active molecules in HD 209 458 b atmosphere obtained by FastChem, with the solar scenario at the top and the C-rich scenario at the bottom.

atmospheric temperature of this planet, leading to H_2S abundantly present only in the lower atmosphere below 10^3 mbar, while the two other cooler planets can maintain the H_2S mixing ratio greater than 10^{-5} even at altitudes up to 10^{-3} mbar (as Fig. 5). These differences in H_2S abundance may affect the retrievability of sulphur in WASP-121 b.

By contrast, as shown by the posterior distributions of HD 209 458 b and HD 189 733 b, the S/O ratio is well constrained and consistent with the ground truth in almost all of our scenarios. Especially the distinction between the S-rich scenario and all the others can be made, despite the absolute change in S/O being small. As shown in Fig. 6, we find that all S-related molecules (H_2S, SH, SO_2, CS, and NS) have increased abundances in the S-rich case (they rise on average by an additional 80 per cent).

In the bottom panel of Fig. 4, we show a breakdown of the spectral contribution for the S-rich case. While SH can reach abundances of up to 10^{-5} in a certain altitude, its contribution to the observed spectra is small. However, H_2S possesses strong spectral features and its abundances variate with changes in S/O, so the molecule plays a key role in the retrievals of the S/O ratio. Additionally, Rustamkulov et al. (2023) has suggested that SO_2 is needed to explain *JWST* observations of WASP-39 b. SO_2 molecular contribution is not included in our analysis as it was not predicted by our chemical model which does not account for photo-chemistry.

In the posterior distribution of the C-rich scenario, the uncertainty of the S/O ratio and metallicity are increased. The distribution of the S/O ratio is broadened slightly and extended to a larger value, while the retrieved results for metallicity tend to extend to a lower level. This is likely due to the lack of H_2O signature in the C-rich case, which limits the recovery of the oxygen abundance and overall degrades the retrieved species to oxygen ratios (see the comparison between the two sub-figures in Fig. 3).

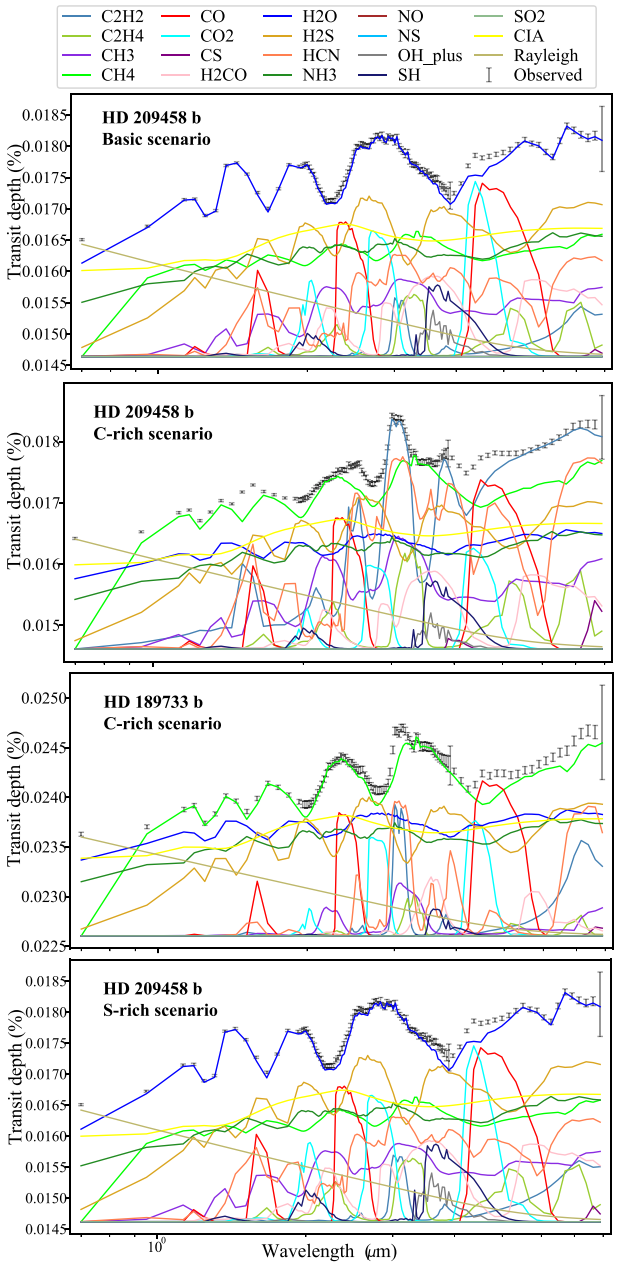

Figure 4. Spectral contributions of various molecules for different cases. Top panel: The basic solar scenario in HD 209 458 b. Top middle panel: The C-rich scenario in HD 209 458 b. Bottom middle panel: The C-rich scenario in HD 189 733 b. Bottom panel: The S-rich scenario in HD 209 458 b.

3.4 N/O ratio

In contrast to the other parameters, the detectability of the nitrogen ratio is difficult. We find that the ratio of N/O is unconstrained in most of our cases, and its retrievability is not enhanced even in the (4) N-rich scenario. However, in a high C/O or high metallicity environment, N can be recovered from the higher abundances of HCN. That is, for the (2) C-rich, (7) high Z, and (8) very high Z scenarios, the N/O ratio converges to the input values.

By checking the abundance of the nitrogen-related molecules (HCN, NH_3, NO, and NS) varying from scenarios (Fig. 7) and the spectral contributions in the top middle panel of Fig. 4, we see that

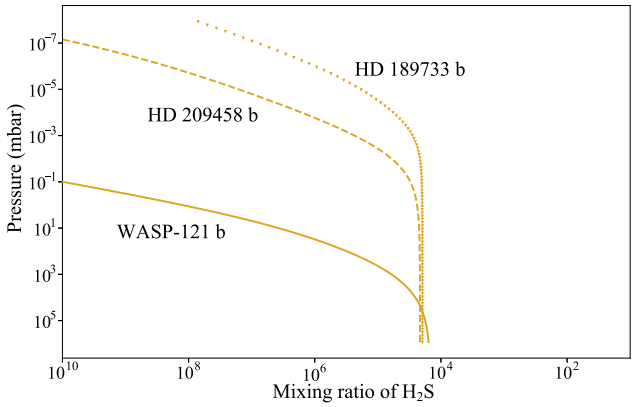

Figure 5. Mixing ratio of H_2S in three exoplanets (S-rich atmosphere).

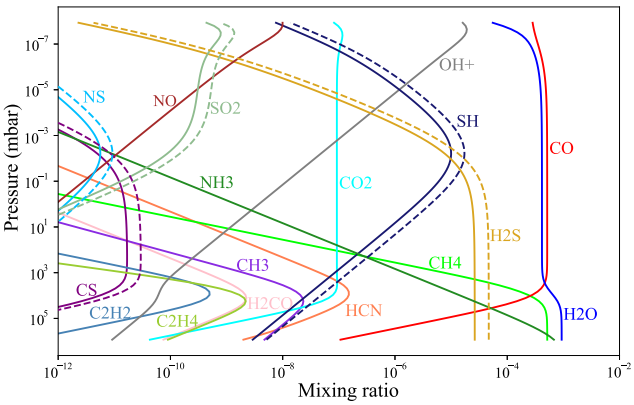

Figure 6. Vertical abundance profiles of active molecules in HD 209 458 b atmospheres with the basic solar scenario (solid lines) and the S-rich scenario (dashed lines).

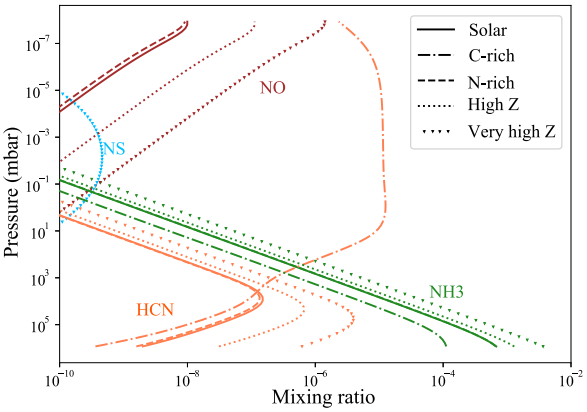

Figure 7. Vertical abundance profiles of N-bearing molecules in HD 209 458 b atmospheres. The species are distinguished by colours, and the different line shapes represent different scenarios.

HCN is the main N contributor to hot-Jupiters atmospheres. This molecule can be picked up at abundances down to 10^{-6} with Ariel and since many of the C-bearing species allow to independently recover the carbon content, the abundance of HCN uniquely defines the N/O ratio (e.g there are little degeneracies between N and C in the high Z case and the C-rich case). So, provided that enough HCN can be produced in an atmosphere, Ariel is able to recover the N/O ratio

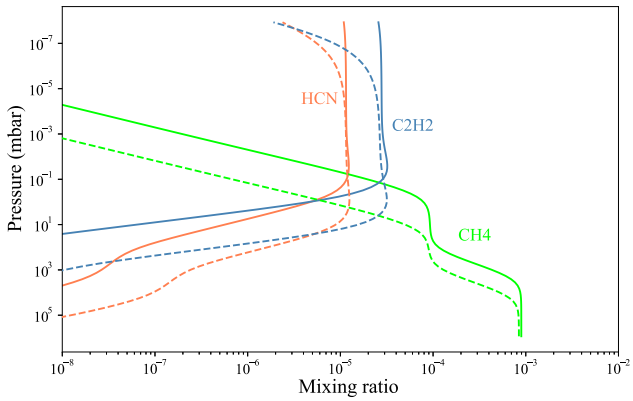

Figure 8. Vertical abundance profiles of three molecules in the C-rich atmosphere for HD 209 458 b (dashed line) and HD 189 733 b (solid line).

of hot Jupiters. For cooler exoplanets, future studies can determine if other tracers such as NH_3, which becomes dominant, can play a similar role.

3.5 Exoplanetary discrepancies

In the C-rich scenario, while the same parameters are used, we can observe some major divergence between the spectra of HD 189 733 b and HD 209 458 b (see Fig. 1). The spectral absorption contributions of multiple species in the wavelength of interest are shown in the top middle and the bottom middle panels of Fig. 4. The absorption features of the CH_4 dominate the continuum in both cases; however, C_2H_2 and HCN have enhanced contributions in the HD 209 458 b atmosphere. This difference is due to the changes in temperatures between the two atmospheres. HD 189 733 b with a cooler effective temperature of 1210 K can maintain more CH_4, while HD 209 458 b which has a higher temperature (1450 K) has C_2H_2 and HCN down to higher pressures. This is reflected in Fig. 8, which shows the vertical abundance profiles of these three molecules in the two planetary atmospheres for the C-rich scenario [see also the results of Heng & Tsai (2016)]. This highlights the non-linear behaviour of atmospheric chemistry and therefore the difficulty in expanding the results of our study to other cases.

4 DISCUSSION

In the previous section, we have demonstrated that the observations with the future mission Ariel will be capable of characterizing the abundance of most critical elemental ratios as well as metallicity in the atmospheres of hot Jupiters within the majority of cases we simulated. Here we discuss in particular the retrieval of N/O from hot Jupiter atmospheres.

As stated in Section 3.4, a carbon-rich or metal-rich environment would improve the retrievability of the N/O ratio. Here we conduct additional experiments and discuss the influence of the C/O and metallicity separately on the constraint of N/O posterior distributions. The following two issues will be addressed.

(i) **How do constraints on N/O vary with carbon-to-oxygen ratio or metallicity?** We tested additional scenarios with interval variations of carbon abundance based on the nitrogen-rich atmospheres, adopting C/O $= 0.2$, 0.55, 0.75, 0.95, and 1.1, separately. Another set of experiments focused on the changes of metallicity from a lower value of 0.5 to a higher value of 7.6 in linear space and extended to larger 15 and 50. This enables more precisely

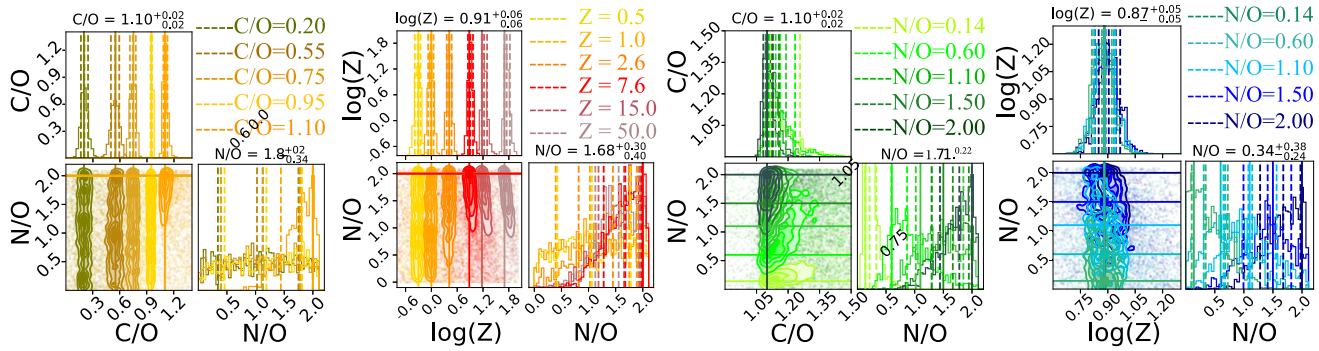

Figure 9. Correlation posterior distributions of N/O, C/O, and metallicity for investigating the changes in N/O constraint occurring under different scenarios. Left-hand panel: The N-rich environments (N/O = 2.0, S/O = 0.028, Z = 1.0) with interval variations of carbon abundance (C/O from 0.2 to 1.1). Centre left-hand panel: The N-rich environments with successively increasing metallicity (Z from 0.5 to 50). Centre right-hand panel: The C-rich environments (C/O = 1.1, S/O = 0.028, Z = 1.0) with different nitrogen abundances (N/O = 0.14, 0.6, 1.1, 1.5, and 2.0). Right-hand panel: The high-Z environments (C/O = 0.55, S/O = 0.028, Z = 7.6) with different nitrogen abundances.

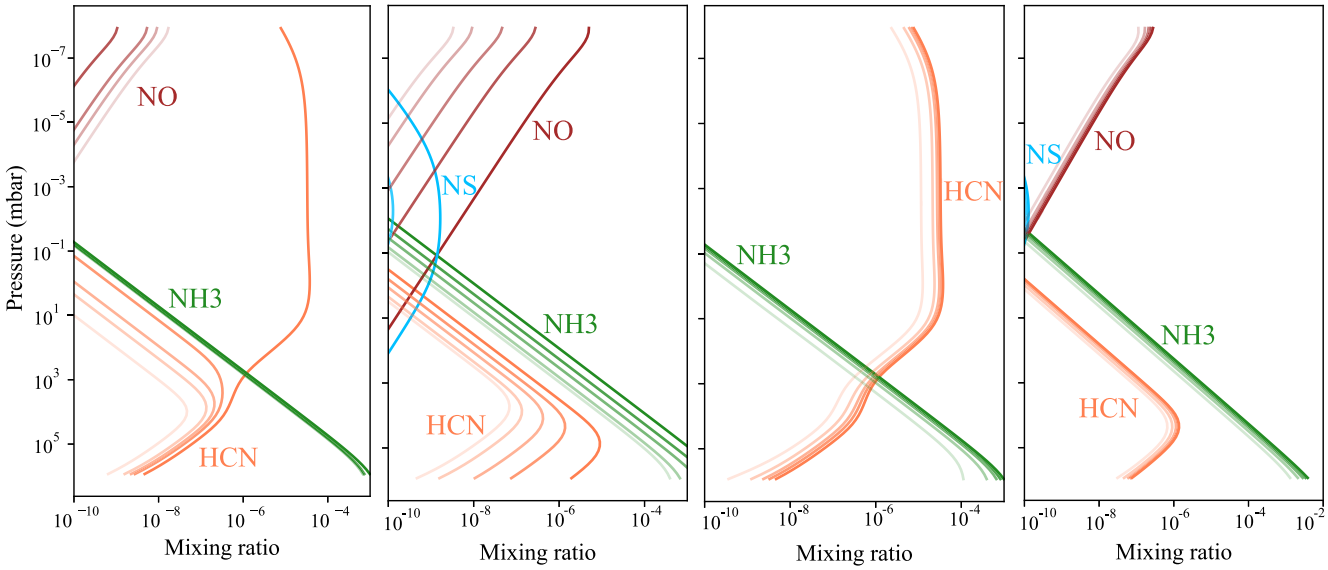

Figure 10. Vertical abundance profile of the nitrogen-bearing molecules with different C/O abundances based on the N-rich scenario (left-hand panel), different metallicities based on the N-rich scenario (centre left-hand panel), different N/O abundances based on the C-rich scenario (centre right-hand panel) and different N/O abundances based on the high Z scenario (right-hand panel). Each species is represented by the same colour, and lighter colours represent lower abundance.

determining the required C/O and metallicity to recover constraints on N/O. The left-hand panel of Fig. 9 shows the posterior distribution of N/O as a function of C/O, and the left-hand panel of Fig. 10 shows the vertical abundances of nitrogen-containing molecules at different carbon contents, with lower C/O ratio being represented as lighter colours. We find that the N/O is well constrained only in the case of C/O = 1.1, implying a sharp change from a low HCN regime to a high HCN regime above C/O ≈ 1. This is also consistent with the molecular profiles, where HCN reaches detectable values only in the highest C/O case. The lack of change in other molecules confirms our earlier interpretation that HCN is the key molecule for Ariel in constraining the element nitrogen in hot Jupiter atmospheres. In comparison, the retrieval of N/O is gradually improved with increasing metallicity as shown in the centre left-hand panel of Fig. 9. This is due to the globally increased abundances of N-bearing molecules, particularly for HCN and NH_3 (see the centre left-hand panel of Fig. 10), which can reach deep atmospheric abundances (> 1 bar) of up to 10^{-4}.

(ii) **Can various N/O be recovered in the C-rich/high-Z environment?** We performed two additional sets of experiments with the variable nitrogen content (N/O = 0.14, 0.6, 1.1, 1.5, and 2.0) in both the C-rich and metal-rich environments. From the posterior distributions in the centre right-hand and the right-hand panels of Fig. 9, Ariel can recover the N/O of a wide range of cases, provided that the C/O or the metallicity of the atmosphere is super-solar. The measurement is difficult, however, and small variations in the N/O ratio cannot be achieved without a high SNR. This is due to the mixing ratio profile of each N-bearing molecule (see the centre right-hand panel for the C-rich and the right-hand panel for the high Z in Fig. 10) remaining relatively close despite changes in the nitrogen abundances.

We note that this study is limited to three cases (HD 209 458 b, HD 189 733 b, and WASP-121 b), which are only three planets amongst the wide range of predicted targets (Edwards & Tinetti 2022) for Ariel. The findings of our article demonstrate the ability to recover accurate metallicity, C/O, S/O ratio, and N/O ratio (in certain

scenarios) in typical hot Jupiters with Ariel, but the conclusions cannot be directly extended to all the targets. For such purpose, future works performing population-level simulations, such as in Changeat et al. (2020), have to be conducted.

Additionally, many simplifications or effects are neglected in this study. In particular, we note that the effects of clouds and hazes are not considered in our simulations, which would definitely affect the retrievability of planetary formation and evolution tracers. Atmospheres are also modeled using simplifying assumptions such as isothermal profiles (Rocchetto et al. 2016), chemical equilibrium chemistry (Drummond et al. 2020; Venot et al. 2020; Moses et al. 2022), or even simplified one-dimensional modelling (Feng et al. 2016; Caldas et al. 2019; MacDonald, Goyal & Lewis 2020; Changeat et al. 2021b; Taylor et al. 2021; Taylor 2022), which in reality would also require additional considerations to extract accurate constraints on elemental abundances. Finally, we only varied the planetary composition one parameter at a time, while in realistic planetary mixtures the different elements do not vary independently from each other (Turrini et al. 2021; Biazzo et al. 2022; Pacetti et al. 2022; Turrini et al. 2022).

It should be noted that our study remains theoretical at present, but upcoming *JWST* data should help to constrain elemental ratios in a number of hot Jupiters, allowing us to refine our analysis using more realistic data.

5 CONCLUSIONS

We have investigated here the ability of the Ariel mission to constrain the metallicity and three important elemental ratios in the atmospheres of hot Jupiters (Tinetti et al. 2021; Turrini et al. 2021, 2022; Pacetti et al. 2022). We have performed retrieval analyses for three representative hot Jupiters, different SNR, and eight atmospheric scenarios. We found that the retrieval of the metallicity and the C/O is driven by the abundance of species such as H_2O, CO, CO_2, CH_4 but also HCN and C_2H_2. The S/O was inferred here solely from the contribution of H_2S and could be well retrieved if the abundance of H_2S was not negligible. Concerning the N/O, the cases we investigated were more complex due to the lack of strong absorption by N-bearing species. We found that in a carbon-rich or a high metallicity environment, the recovery of HCN would enable constraining the N:O ratio. This possibility can however be challenging in the case of solar abundances and for other chemical regimes. Additional experiments were carried out to discuss the sensitivity of the N/O to metallicity and C/O, indicating that N/O could only be retrieved where C/O exceeded 1 (there is a sharp regime change in the chemistry for C/O $>$ 1) or for increased metallicity (the effect here is more gradual). We highlight that our work provides a simplified attempt to investigate the recovery of elemental ratios with next-generation telescopes. Many assumptions will have to be refined in the future to extend the scope of this study to a wider range of exoplanets and account for more realistic atmospheres. Despite these limitations, the results from the retrieval experiments reported here support the capability of the Ariel telescope to detect formation and evolution tracers in a large sample of hydrogen-rich atmospheres.

ACKNOWLEDGEMENTS

DT acknowledges the support of the Italian National Institute of Astrophysics (INAF) through the INAF Main Stream project 'Ariel and the astrochemical link between circumstellar discs and planets' (CUP: C54I19000700005), of the Italian Space Agency (ASI) through the ASI-INAF contract no. 2021-5-HH.0, and of the European Research Council via the Horizon 2020 Framework Programme ERC Synergy 'ECOGAL' Project GA-855130.

DATA AVAILABILITY

The data underlying this article are available in the article and in its online supplementary material.

REFERENCES

Adam A. Y., Yachmenev A., Yurchenko S. N., Jensen P., 2019, J. Phys. Chem., 123, 4755
Addison B. et al., 2019, PASP, 131, 115003
Al-Refaie A. F., Yachmenev A., Tennyson J., Yurchenko S. N., 2015, MNRAS, 448, 1704
Al-Refaie A. F., Changeat Q., Waldmann I. P., Tinetti G., 2021, ApJ, 917, 37
Al-Refaie A. F., Changeat Q., Venot O., Waldmann I. P., Tinetti G., 2022b, ApJ, 932, 123
Asplund M., Grevesse N., Sauval A. J., Scott P., 2009, Annual Review of Astronomy and Astrophysics, 47, 481
Azzam A. A. A., Tennyson J., Yurchenko S. N., Naumenko O. V., 2016, MNRAS, 460, 4063
Barber R. J., Strange J. K., Hill C., Polyansky O. L., Mellau G. C., Yurchenko S. N., Tennyson J., 2013, MNRAS, 437, 1828
Ben-Yami M., Madhusudhan N., Cabot S. H. C., Constantinou S., Piette A., Gandhi S., Welbanks L., 2020, ApJ, 897, L5
Bernath P. F., 2020, J. Quant. Spectrosc. Radiat. Transfer, 240, 106687
Biazzo K. et al., 2022, A&A, 664, A161
Birkby J. L., de Kok R. J., Brogi M., de Mooij E. J. W., Schwarz H., Albrecht S., Snellen I. A. G., 2013, MNRAS, 436, L35
Blumenthal S. D., Mandell A. M., Hébrard E., Batalha N. E., Cubillos P. E., Rugheimer S., Wakeford H. R., 2018, ApJ, 853, 138
Bonomo A. S. et al., 2017, A&A, 602, A107
Bouchy F. et al., 2005, A&A, 444, L15
Bourgalais J. et al., 2020, ApJ, 895, 77
Bourrier V. et al., 2020, A&A, 635, A205
Brogi M., Line M. R., 2019, AJ, 157, 114
Brown T. M., 2001, ApJ, 553, 1006
Cabot S. H. C., Madhusudhan N., Hawker G. A., Gandhi S., 2018, MNRAS, 482, 4422
Cabot S. H., Madhusudhan N., Welbanks L., Piette A., Gandhi S., 2020, MNRAS, 494, 363
Caldas A., Leconte J., Selsis F., Waldmann I. P., Bordé P., Rocchetto M., Charnay B., 2019, A&A, 623, A161
Changeat Q., Hou Yip K., 2023, RAS Techniques and Instruments, 2, 45
Changeat Q., Edwards B., Waldmann I. P., Tinetti G., 2019, ApJ, 886, 39
Changeat Q., Al-Refaie A., Mugnai L. V., Edwards B., Waldmann I. P., Pascale E., Tinetti G., 2020, AJ, 160, 80
Changeat Q., Edwards B., Al-Refaie A. F., Tsiaras A., Waldmann I. P., Tinetti G., 2021a, Exp. Astron., 53, 391
Changeat Q., Al-Refaie A. F., Edwards B., Waldmann I. P., Tinetti G., 2021b, ApJ, 913, 73
Changeat Q. et al., 2022, ApJS, 260, 3
Charbonneau D., Brown T. M., Latham D. W., Mayor M., 1999, ApJ, 529, L45
Chubb K. L., Tennyson J., Yurchenko S. N., 2020, MNRAS, 493, 1531
Chubb K. L. et al., 2021, A&A, 646, A21
Coles P. A., Yurchenko S. N., Tennyson J., 2019, MNRAS, 490, 4638
Cridland A. J., Eistrup C., Van Dishoeck E. F., 2019, A&A, 627, A127
Cubillos P. E., Fossati L., Koskinen T., Young M. E., Salz M., France K., Sreejith A., Haswell C. A., 2020, AJ, 159, 111
de Kok R. J., Brogi M., Snellen I. A. G., Birkby J., Albrecht S., de Mooij E. J. W., 2013, A&A, 554, A82
Deming D. et al., 2013, ApJ, 774, 95
Drummond B. et al., 2020, A&A, 636, A68
Edwards B., Tinetti G., 2022, AJ, 164, 15
Edwards B., Mugnai L., Tinetti G., Pascale E., Sarkar S., 2019, AJ, 157, 242

Eistrup C., Walsh C., Van Dishoeck E. F., 2016, A&A, 595, A83
Eistrup C., Walsh C., van Dishoeck E. F., 2018, A&A, 613, A14
Evans T. M. et al., 2016, ApJ, 822, L4
Evans T. M. et al., 2018, AJ, 156, 283
Feng Y. K., Line M. R., Fortney J. J., Stevenson K. B., Bean J., Kreidberg L., Parmentier V., 2016, ApJ, 829, 52
Feng Y. K., Robinson T. D., Fortney J. J., Lupu R. E., Marley M. S., Lewis N. K., Macintosh B., Line M. R., 2018, AJ, 155, 200
Feroz F., Hobson M. P., Bridges M., 2009, MNRAS, 398, 1601
Foreman-Mackey D., 2016, J. Open Source Softw., 1, 24
Giacobbe P. et al., 2021, Nature, 592, 205
Gibson N. P. et al., 2020, MNRAS, 493, 2215
Gorman M. N., Yurchenko S. N., Tennyson J., 2019, MNRAS, 490, 1652
Greene T. P., Line M. R., Montero C., Fortney J. J., Lustig-Yaeger J., Luther K., 2016, ApJ, 817, 17
Heng K., Tsai S.-M., 2016, ApJ, 829, 104
Henry G. W., Marcy G. W., Butler R. P., Vogt S. S., 1999, ApJ, 529, L41
Hodges J. N., Bernath P. F., 2017, ApJ, 840, 81
Hoeijmakers H. J. et al., 2020, A&A, 641, A123
Keles E. et al., 2019, MNRAS, 489, L37
Knierim H., Shibata S., Helled R., 2022, A&A, 665, L5
Kolecki J. R., Wang J., 2022, AJ, 164, 87
Lampón M. et al., 2020, A&A, 636, A13
Lampón M. et al., 2021, A&A, 647, A129
Li G., Gordon I. E., Rothman L. S., Tan Y., Hu S.-M., Kassi S., Campargue A., Medvedev E. S., 2015, ApJS, 216, 15
MacDonald R. J., Madhusudhan N., 2017, MNRAS, 469, 1979
MacDonald R. J., Goyal J. M., Lewis N. K., 2020, ApJ, 893, L43
Madhusudhan N., 2012, ApJ, 758, 36
Madhusudhan N., Seager S., 2009, ApJ, 707, 24
Mant B. P., Yachmenev A., Tennyson J., Yurchenko S. N., 2018, MNRAS, 478, 3220
Marty B. et al., 2009, Exp. Astron., 23, 947
Merritt S. R. et al., 2021, MNRAS, 506, 3853
Mikal-Evans T. et al., 2023, The Astrophysical Journal Letters, 943, L17
Mordasini C., van Boekel R., Mollière P., Henning T., Benneke B., 2016, ApJ, 832, 41
Moses J. I., Madhusudhan N., Visscher C., Freedman R. S., 2012, ApJ, 763, 25
Moses J. I., Tremblin P., Venot O., Miguel Y., 2022, Exp. Astron., 53, 279
Mousis O. et al., 2018, Planet. Space Sci., 155, 12
Mugnai L. V., Pascale E., Edwards B., Papageorgiou A., Sarkar S., 2020, Exp. Astron., 50, 303
Mugnai L. V., Al-Refaie A., Bocchieri A., Changeat Q., Pascale E., Tinetti G., 2021, AJ, 162, 288
Nowak M. et al., 2020, A&A, 633, A110
Öberg K. I., Murray-Clay R., Bergin E. A., 2011, ApJ, 743, L16
Owen T., Encrenaz T., 2003, Space Sci. Rev., 106, 121
Pacetti E. et al., 2022, ApJ, 937, 36
Paulose G., Barton E. J., Yurchenko S. N., Tennyson J., 2015, MNRAS, 454, 1931
Polyansky O. L., Kyuberis A. A., Zobov N. F., Tennyson J., Yurchenko S. N., Lodi L., 2018, MNRAS, 480, 2597
Qu Q., Yurchenko S. N., Tennyson J., 2021, MNRAS, 504, 5768
Richard C. et al., 2012, J. Quant. Spectrosc. Radiat. Transfer, 113, 1276
Rocchetto M., Waldmann I. P., Venot O., Lagage P. O., Tinetti G., 2016, ApJ, 833, 120
Rustamkulov Z. et al., 2023, Nature, 614, 659
Scott P. et al., 2015a, A&A, 573, A25
Scott P., Asplund M., Grevesse N., Bergemann M., Sauval A. J., 2015b, A&A, 573, A26
Shibata S., Helled R., 2022, ApJ, 926, L37
Shibata S., Helled R., Ikoma M., 2020, A&A, 633, A33
Shibata S., Helled R., Ikoma M., 2022, A&A, 659, A28
Sing D. K. et al., 2016, Nature, 529, 59
Sing D. K. et al., 2019, AJ, 158, 91
Snellen I. A. G., de Kok R. J., de Mooij E. J. W., Albrecht S., 2010, Nature, 465, 1049
Stock J. W., Kitzmann D., Patzer A. B. C., Sedlmayr E., 2018, MNRAS, 479, 865
Swain M. R., Vasisht G., Tinetti G., 2008, Nature, 452, 329
Swain M. R. et al., 2009, ApJ, 704, 1616
Taylor J., 2022, MNRAS, 513, L20
Taylor J., Parmentier V., Line M. R., Lee E. K. H., Irwin P. G. J., Aigrain S., 2021, MNRAS, 506, 1309
The JWST Transiting Exoplanet Community Early Release Science Team et al., 2023, Nature, 614, 649
Thompson M. A., Telus M., Schaefer L., Fortney J. J., Joshi T., Lederman D., 2021, Nature Astron., 5, 575
Tinetti G. et al., 2007, Nature, 448, 169
Tinetti G. et al., 2018, Exp. Astron., 46, 135
Tinetti G. et al., 2021, Ariel Definition Study Report. ESA Document ESA/SCI(2020)1, preprint (arXiv:2104.04824)
Tsiaras A., Waldmann I. P., Rocchetto M., Varley R., Morello G., Damiano M., Tinetti G., 2016, ApJ, 832, 202
Turrini D. et al., 2021, ApJ, 909, 40
Turrini D. et al., 2022, Exp. Astron., 53, 225
Underwood D. S., Tennyson J., Yurchenko S. N., Huang X., Schwenke D. W., Lee T. J., Clausen S., Fateev A., 2016, MNRAS, 459, 3890
Venot O., Hébrard E., Agúndez M., Decin L., Bounaceur R., 2015, A&A, 577, A33
Venot O., Cavalié T., Bounaceur R., Tremblin P., Brouillard L., Lhoussaine Ben Brahim R., 2020, A&A, 634, A78
Vidal-Madjar A. et al., 2004, ApJ, 604, L69
Vidal-Madjar A. et al., 2013, A&A, 560, A54
Wang F., Fan X., Wang H., Pan Y., Shen Y., Lu X., Du X., Lin S., 2021, Appl. Sci., 11, 5508
Wong A., Yurchenko S. N., Bernath P., Müller H. S. P., McConkey S., Tennyson J., 2017, MNRAS, 470, 882
Wyttenbach A., Ehrenreich D., Lovis C., Udry S., Pepe F., 2015, A&A, 577, A62
Yip K. H., Changeat Q., Nikolaou N., Morvan M., Edwards B., Waldmann I. P., Tinetti G., 2021, AJ, 162, 195
Yurchenko S. N., Amundsen D. S., Tennyson J., Waldmann I. P., 2017, A&A, 605, A95
Yurchenko S. N., Bond W., Gorman M. N., Lodi L., McKemmish L. K., Nunn W., Shah R., Tennyson J., 2018, MNRAS, 478, 270
Yurchenko S. N., Mellor T. M., Freedman R. S., Tennyson J., 2020, MNRAS, 496, 5282

APPENDIX A: RETRIEVALS OF SCATTERED SPECTRA

To demonstrate the reliability of the retrievals with non-scattered observations, we repeat some retrievals with scattered data as the observed spectra, based on the case of five combined observations to the basic solar scenario in HD 209458 b. We applied a Gaussian scatter to the spectra by using the true value as mean and the simulated noise as variance. As we can see from the posterior distributions of the scattered and non-scattered spectra in Fig. A1, the distribution results of each free parameter are approximate in general, and almost all of them can be fitted to the ground truth for each set of data, although the retrieved results have a slight deviation due to the influence of noise. Therefore, for the repeatability and reproducibility of our experiments, the non-scatter data are adopted in the simulation, just as discussed in Section 2.3.

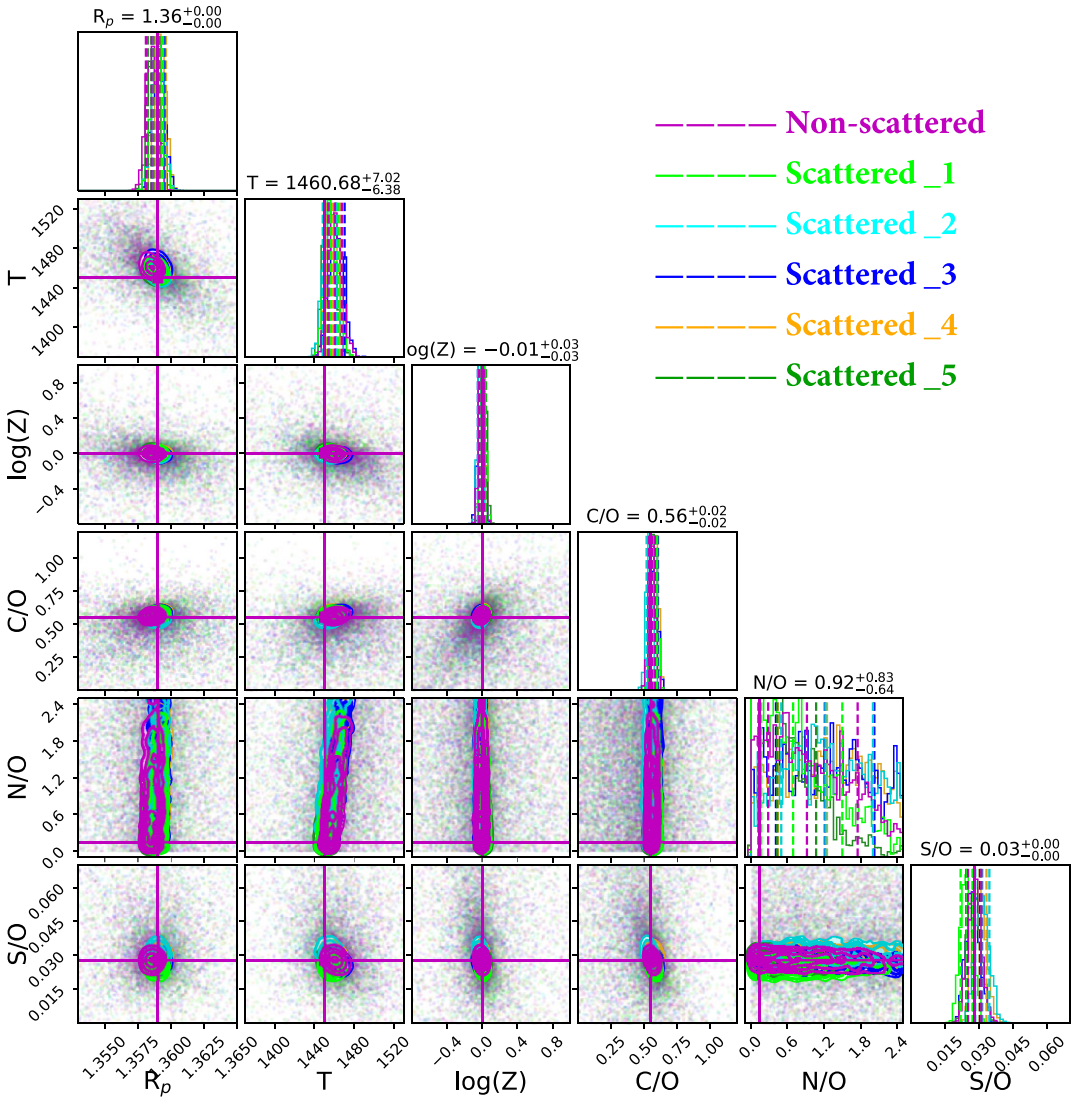

Figure A1. Posterior distributions with scattered and non-scattered observations.

APPENDIX B: POSTERIOR DISTRIBUTIONS

In this appendix, we exhibit the posterior results of additional retrieval simulations in the corner plots with uniform parameters and priors. Fig. B1 reveals the fitted results with the eight originally adopted atmospheric scenarios for HD 209458 b with 20 combined transits, in order to discuss the effect of the number of observations on retrieval uncertainty. Likewise, Fig. B2 displays the posteriors for HD 189733 b combined with five transits, as well as Fig. B3 for WASP-121 b, to discuss the results of targeting a different exoplanet under the equivalent of Fig. 2.

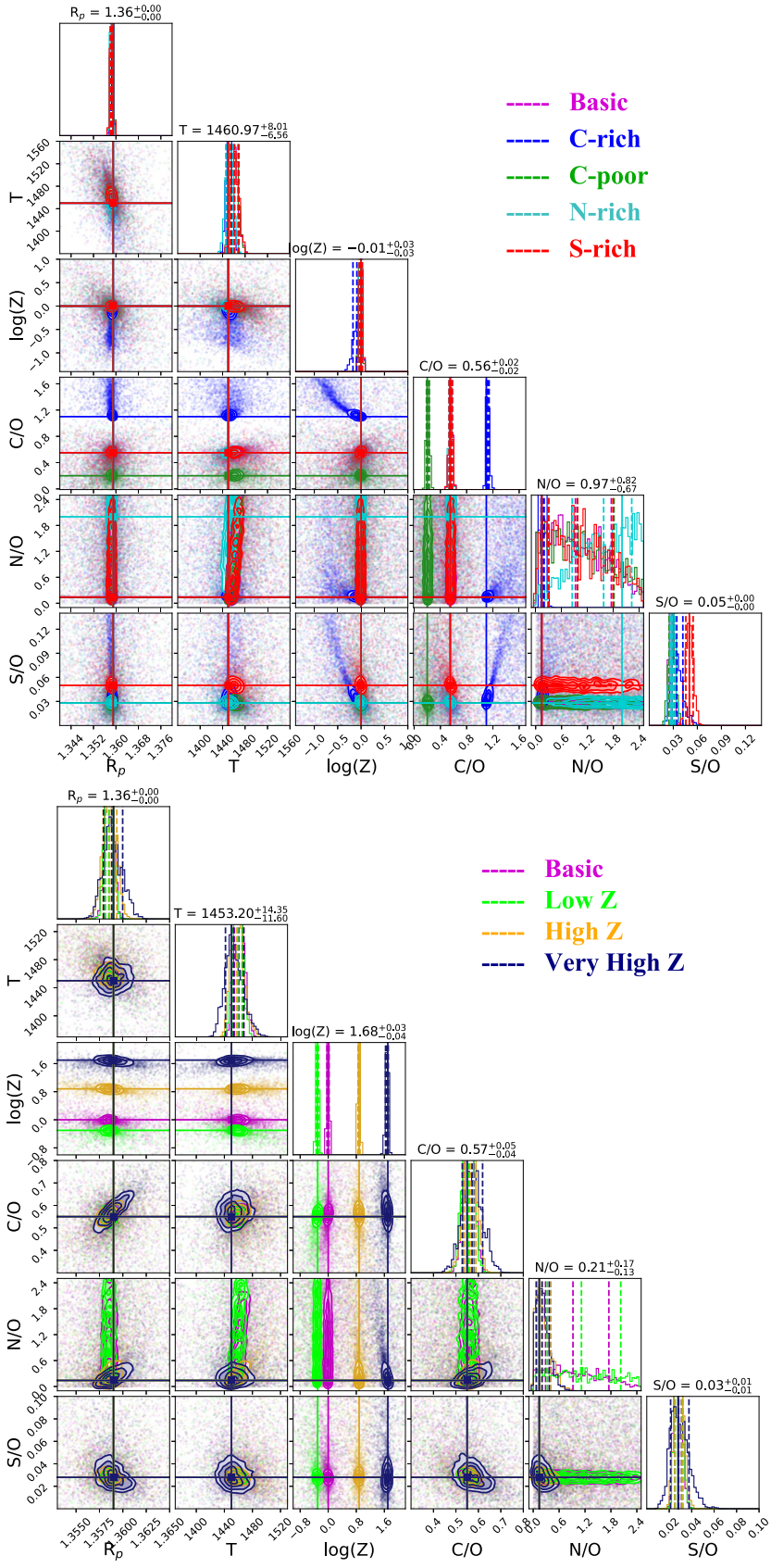

Figure B1. Posterior distributions for the eight scenarios in the case of HD 209458 b when we combined 20 transit observations obtained with Ariel. Scenarios 1, 2, 3, 4, and 5 are plotted at the top, and scenarios 1, 6, 7, and 8 at the bottom.

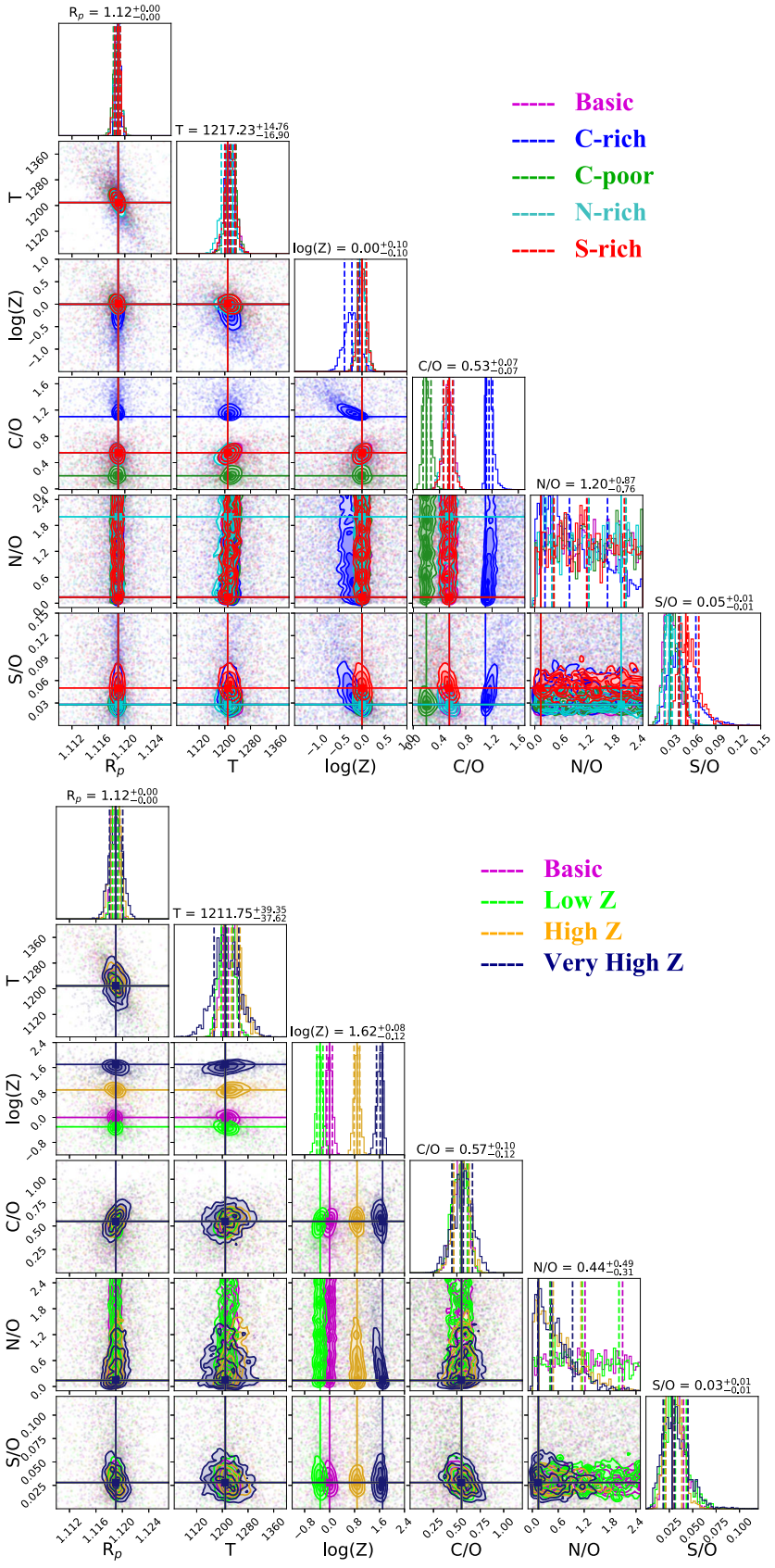

Figure B2. Posterior distributions for the eight scenarios in the case of HD 189733 b when we combined five transit observations obtained with Ariel. Scenarios 1, 2, 3, 4, and 5 are plotted at the top, and scenarios 1, 6, 7, and 8 at the bottom.

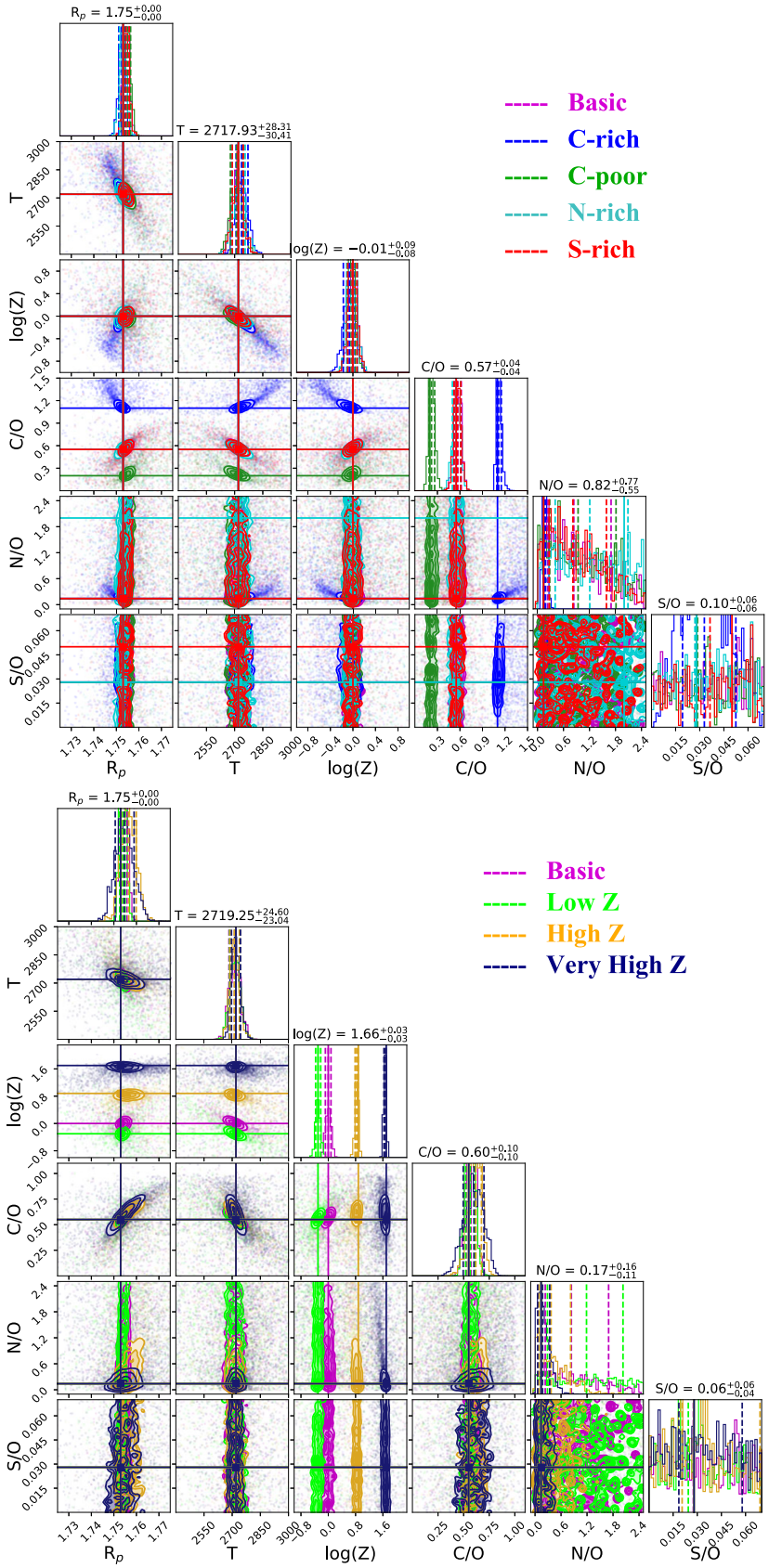

Figure B3. Posterior distributions for the eight scenarios in the case of WASP-121 b when we combined five transit observations obtained with Ariel. Scenarios 1, 2, 3, 4, and 5 are plotted at the top, and scenarios 1, 6, 7, and 8 at the bottom.

APPENDIX C: MEDIAN AND CREDIBLE RANGES

Here we list the median and 1σ credible ranges of the retrieved parameters in Table. C1 according to our retrieval results of posteriors, with 5 and 20 simulated transits separately. The table is used to explain the influence of multiple observations on the uncertainty of retrieval parameters described in Section 3.

Table C1. Median and 1σ credible ranges for element-to-O ratios and metallicity from posteriors when 5 and 20 transits were observed by Ariel for all eight scenarios of HD 209458 b.

N_t	5 observations				20 observations			
Scenarios	Log(Z)	C/O	N/O	S/O	Log(Z)	C/O	N/O	S/O
Basic	$-0.00^{+0.05}_{-0.07}$	$0.55^{+0.05}_{-0.05}$	$1.03^{+0.71}_{-0.70}$	$0.03^{+0.01}_{-0.01}$	$-0.01^{+0.03}_{-0.03}$	$0.56^{+0.02}_{-0.02}$	$0.88^{+0.70}_{-0.63}$	$0.03^{+0.00}_{-0.00}$
C-rich	$-0.22^{+0.17}_{-0.21}$	$1.16^{+0.10}_{-0.05}$	$0.21^{+0.12}_{-0.07}$	$0.05^{+0.03}_{-0.02}$	$-0.01^{+0.08}_{-0.08}$	$1.12^{+0.02}_{-0.02}$	$0.16^{+0.04}_{-0.03}$	$0.03^{+0.01}_{-0.01}$
C-poor	$-0.01^{+0.05}_{-0.06}$	$0.21^{+0.04}_{-0.04}$	$0.99^{+0.71}_{-0.66}$	$0.03^{+0.01}_{-0.01}$	$-0.01^{+0.03}_{-0.03}$	$0.21^{+0.02}_{-0.02}$	$0.89^{+0.72}_{-0.59}$	$0.03^{+0.00}_{-0.00}$
N-rich	$-0.02^{+0.07}_{-0.06}$	$0.55^{+0.04}_{-0.05}$	$1.02^{+0.72}_{-0.63}$	$0.03^{+0.01}_{-0.01}$	$-0.01^{+0.03}_{-0.03}$	$0.55^{+0.02}_{-0.02}$	$1.32^{+0.54}_{-0.63}$	$0.03^{+0.00}_{-0.00}$
S-rich	$-0.01^{+0.06}_{-0.07}$	$0.55^{+0.04}_{-0.05}$	$0.96^{+0.79}_{-0.63}$	$0.05^{+0.01}_{-0.01}$	$-0.01^{+0.03}_{-0.03}$	$0.56^{+0.02}_{-0.02}$	$0.89^{+0.77}_{-0.60}$	$0.03^{+0.00}_{-0.00}$
Low Z	$-0.31^{+0.07}_{-0.07}$	$0.55^{+0.05}_{-0.05}$	$0.98^{+0.80}_{-0.64}$	$0.03^{+0.01}_{-0.01}$	$-0.31^{+0.03}_{-0.03}$	$0.55^{+0.03}_{-0.02}$	$1.04^{+0.71}_{-0.67}$	$0.03^{+0.00}_{-0.00}$
High Z	$0.87^{+0.05}_{-0.05}$	$0.57^{+0.05}_{-0.05}$	$0.34^{+0.38}_{-0.24}$	$0.03^{+0.01}_{-0.01}$	$0.88^{+0.03}_{-0.03}$	$0.56^{+0.03}_{-0.03}$	$0.20^{+0.19}_{-0.13}$	$0.03^{+0.00}_{-0.00}$
Very high Z	$1.65^{+0.06}_{-0.07}$	$0.59^{+0.08}_{-0.07}$	$0.32^{+0.28}_{-0.22}$	$0.03^{+0.02}_{-0.01}$	$1.68^{+0.04}_{-0.05}$	$0.57^{+0.05}_{-0.05}$	$0.19^{+0.18}_{-0.12}$	$0.03^{+0.01}_{-0.01}$

This paper has been typeset from a TEX/LATEX file prepared by the author.